AIChE

A Promising Method for Electrodeposition of Aluminium on Stainless Steel in Ionic Liquid

Guikuan Yue
Institute of Process Engineering, Chinese Academy of Sciences, Beijing 100190, P.R. China

College of Chemistry and Chemical Engineering, Graduate University of Chinese Academy of Sciences, Beijing 100049, P.R. China

Suojiang Zhang, Yanli Zhu, Xingmei Lu, and Shucai Li
Institute of Process Engineering, Chinese Academy of Sciences, Beijing 100190, P.R. China

Zengxi Li
College of Chemistry and Chemical Engineering, Graduate University of Chinese Academy of Sciences, Beijing 100049, P.R. China

DOI 10.1002/aic.11698
Published online January 22, 2009 in Wiley InterScience (www.interscience.wiley.com).

A promising method for aluminium deposition was proposed by using $AlCl_3$/[bmim]Cl (1-butyl-3-methylimidazolium chloride) ionic liquid as electrolyte. By using this novel method, the volatile and flammable organic solvent systems and the high corrosive inorganic molten salts with high temperature can be substituted, and the deposit microstructure can be easily adjusted by changing the current density, temperature and electrolyte composition. The study was performed by means of galvano-static electrolysis and the optimum operating conditions were determined based on the systematic studies of the effects of current density, temperature, molar ratio of $AlCl_3$ to [bmim]Cl, stirring speed and deposition time on the quality of deposited coatings. The electrical conductivities of electrolytes were also investigated as a function of temperature (298–358 K) and molar ratio of $AlCl_3$ to [bmim]Cl (from 0.1:1 to 2.0:1). Dense, bright and adherent aluminium coatings were obtained over a wide range of temperature (298–348 K), current densities (8–44 mA/cm^2) and molar ratio (1.6:1–2.0:1). Results from the analysis of crystal structure show that all of the electrodeposits exhibit a preferred (200) crystallographic orientation. Temperature has significant influence on the crystallographic orientation and there does not appear to be an apparent impact of current density on it. Analyses of the chronoamperograms indicate that the deposition process of aluminium on stainless steel was controlled by three-dimension nucleation with diffusion-controlled growth and there is a conversion from progressive nucleation to instantaneous nucleation.
 AIChE J, 55: 783–796, 2009
Keywords: ionic liquid, electrodeposition, aluminium, stainless steel, nucleation, orientation

Introduction

It is well known that coating of aluminium (Al) is widely used because of its excellent corrosion resistance, decorativeness and physicochemical properties. Nowadays, various

Correspondence concerning this article should be addressed to S. Zhang at sjzhang@home.ipe.ac.cn.

technologies are available for coating of Al, such as hot dipping,[1,2] thermal spraying,[3] sputter deposition,[4,5] vapor deposition[6,7] and electrodeposition.[8,9] Compared with other procedures, the electrodeposition method is a valuable technology because of its advantages such as mild conditions, easy operation, uniform thickness distribution and adjustable microstructure of the deposited layers. However, the larger negative standard potential of Al/Al(III) couple (−1.67 V vs. NHE) makes the electrodeposition of Al impossible in aqueous solutions owing to a massive hydrogen evolution at the cathode. To solve the above problems, organic aprotic solvents and molten salts have been studied for Al electrodeposition. Although a lot of progresses have been made, there are still many disadvantages for developing competitive coating process of Al.

Three typical kinds of organic solvents are used for electrodeposition of Al: aromatic hydrocarbons,[10–12] dimethylsulfone[13–16] and ethers.[17–21] At present, only two commercial processes on the basis of organic solvents are available for electroplating of Al: SIGAL[10,22] and REAl[23,24] processes. Although high quality Al coating can be obtained by these processes, because of their relatively narrow electrochemical window, low conductivity, low solubility of aluminium salts, higher volatility and flammability, the applications of these organic solvent systems in electrodeposition of Al are limited.

High-temperature inorganic molten salts, such as NaCl-KCl,[25] $AlCl_3$-NaCl,[26,27] and $AlCl_3$-NaCl-KCl[28–30] have been extensively studied and applied for the electrodeposition of Al. However, their highly corrosive natures bring great difficulties for finding container materials that can withstand chemical attack by the melts,[31] and the temperature is very high. Therefore, it is a dream to find mild coating systems.

Over the last decades, aluminium plating in the room temperature molten salts (also called ionic liquids-ILs), has received considerable attention. In the early 1950s, it was first reported by Hurley and Wier[32] that Al can be electrodeposited based on ethylpyridinium chloride/$AlCl_3$ electrolytes. Since then, the development of RTILs has provided a promising alternative method for electrodeposition of Al. They have the merits of both aprotic organic electrolytes and high temperature molten salts. As a replacement, the RTILs have superior features, such as good chemical and thermal stability, low melting points with negligible vapor pressure, high electrical conductivity, and wide electrochemical window of about 4.0 V, which overcome the disadvantages of traditional process. Owing to nonvolatility, they are appropriate for electrodeposition at a range of temperatures, so phenomena such as nucleation, surface diffusion and crystallization associated with the electrodeposition of metals can be accelerated at enhanced temperatures. Furthermore, the process can be easily operated because ionic liquids are nonflammable and nonvolatile if kept below the thermal decomposition temperature. Therefore, the developments of RTILs resulted in another potential approach for Al electrodeposition.

From the 1980s, electrodeposition of Al from $AlCl_3$ based ILs were intensively and systematically studied.[9,33–48] These ILs are mixtures of aluminium chloride and an organic halide (RX) and display adjustable Lewis acidity over a wide range of the molar ratio of $AlCl_3$ to RX.[49] Previous studies show that electrodeposition of Al can only be performed in acidic electrolytes, in which the electroactive $Al_2Cl_7^-$, the only reducible aluminium containing species, are responsible for the electrodeposition according to the following reaction[47]:

$$4Al_2Cl_7^- + 3e^- \rightarrow Al + 7AlCl_4^- \quad (1)$$

Recent studies have shown that even nano-crystalline aluminum deposits can be obtained from $AlCl_3$ based ionic liquid.[50,51] Although these ILs can be used to deposit Al in high quality, a commercial process has not yet been established. Dry air would presumably be sufficient for a technical process. For ionic liquids with large halide concentrations the breakdown of metal oxides on electrode surfaces is prevalent and it is easier for ILs with chloride ions which can acted as good ligands for the dissolving metal ions.[52] This means that an Al sacrificial counter electrode could be employed, which ensures that aluminium concentrations in electrolyte remain approximately steady. It also makes it smaller that the overpotential required to drive the deposition process. However, the electrodeposition was usually performed on limited substrates such as platinum,[35,44] tungsten,[35,37,53] gold,[43,54] copper,[41,55] and glass carbon.[35] Electrodeposition of Al on stainless steel is hardly investigated and it would be very interesting and important to electrodeposit Al on stainless steel.

This work focuses on the studies of Al deposition process based on Lewis acidic $AlCl_3$/[bmim]Cl ILs. The purpose of present work is to electrodeposit dense, bright and adherent Al layers on stainless steel by galvano-static technique. This electrolyte is easy to prepare and relatively simple to handle under dry gas condition. Because there is lack of the conductivity data of this electrolyte and the conductivity is an important factor for the electrodeposition applications, the electrical conductivities of $AlCl_3$/[bmim]Cl were investigated as a function of electrolyte composition and temperature, and analyzed using appropriate theoretical models. The optimum deposition conditions for the Al electrodeposition in these electrolytes also have been determined based on systematic studies of the effects of deposition parameters such as current density, temperature, molar ratio of $AlCl_3$/[bmim]Cl, stirring speed and deposition time. We are especially interested in the electrodeposition of Al on stainless steel substrates due to the practical importance. Our work aims to explore the possibility of using $AlCl_3$/[bmim]Cl ionic liquids as potential electrolytes for Al-plating and provide an alternative for the commercial processes.

Experimental

Preparation of ionic liquid-based electrolyte system

The electrolyte preparation and subsequent electrodepositing were both conducted in an electrolytic cell with a jacket under a dry nitrogen atmosphere. Electrodeposition of Al was studied in a Lewis acidic ionic liquid based on $AlCl_3$ and [bmim]Cl. [bmim]Cl was synthesized in our laboratory. Anhydrous $AlCl_3$ (powder) obtained from Beijing Chemical Reagents Company, without further purification, was used as the initial source of Al. The electrolyte was carefully prepared by mixing precise quantities of $AlCl_3$ and [bmim]Cl in the dry electrolytic cell at ambient temperature. Because the mixing process was exothermic, $AlCl_3$ was slowly added into

[bmim]Cl in small quantities at a time. [bmim]Cl and anhydrous $AlCl_3$ were weighted precisely to make sure the electrolyte was Lewis acidic, i.e., the mol quantity of anhydrous $AlCl_3$ was excessive because Al could not be electrodeposited in basic liquids. After carefully mixing [bmim]Cl with $AlCl_3$, the obtained electrolyte was stirred for several hours and then slowly heated to the predetermined temperatures. In addition, the electrolyte was used without further purification so that the electrodeposition of Al could be investigated in the conditions easily transferable to the industry.

Measurements of electrical conductivities

Electrical conductivity of electrolytes is one of the most important physicochemical properties for electrodeposition application. The conductivities of ILs were measured by a DDS-307 conductivity meter. Electrode constant of the meter was determined by calibration before and after each sample measurement with 0.1 mol/L KCl solution at 298 K and was $1.021 \pm 0.002\ cm^{-1}$.

The measurements were conducted in an electrolytic cell with a jacket under a dry nitrogen atmosphere, using continuous magnetic stirring. Precise quantities of anhydrous $AlCl_3$ were added to [bmim]Cl at different mole fraction, and then the electrolyte was kept at the constant temperature with an accuracy ± 0.1 K for about 2 h until the conductivity was approximately unchanged. Here, the feeding was repeated.

Electrodeposition in ionic liquid

All the experiments were conducted using a three-electrode cell. Al plate (Beijing Chemical Reagents Company, $\geq$99.0%), stainless steel plate and ultra-pure Al wire (Beijing Mountain Technical Development Center For Non-Ferrous Metals, 99.999%) were used as counter electrode, working electrode, and reference electrode, respectively. The distance between the cathode and the anode was about 2.0 cm. Al plate was dipped in NaOH, rinsed with deionized water, followed by acetone and then dried before use; stainless steel was immerged in boiling NaOH, dipped in 20–30% HCl (by volume), washed with deionized water and finally dried. Before use, the working electrodes were mechanically polished with sand paper, treated with a dilute mixture of hydrochloric acid (37%) and sulfuric acid (98%), rinsed with deionized water, and finally immersed into dichloromethane for degreasing. After completing the pretreatments, the electrodes were assembled for immediate use.

Electrochemical measurements were performed using a CHI660C Electrochemical Workstation controlled with a personal computer. The depositions were performed under a predetermined experimental temperature. The cell was maintained under an inert atmosphere by introducing nitrogen into the cell at a constant flow rate. The electrolyte was stirred at a constant speed. The main technique used in this study was galvano-static electrolysis. Post-electrolysis treatment was critical: After each deposition experiment, excess IL was removed from the sample by washing in absolute alcohol; then the sample was rinsed with deionized water and dried with cool air.

Analysis and characterization of the aluminium coatings

Surface morphology of the films was examined with emission scanning electron microscope (SEM, JSM-6700F). The compositional analysis of the deposits was confirmed by energy dispersive analysis by X-ray (EDAX, Oxford INCA300). The crystal structure was studied on an X'Pert PRO (PANalytical) X-ray diffractometer with Cu Kα radiation. The adherence of the deposited Al coatings was simply tested by bending the samples.

Current efficiency calculation is based on the weight difference of the cathode before and after electrolysis and the theoretical yield of Al deposits under given conditions, shown by Eq. 2:

$$\text{Current efficiency } (\%) = \frac{3\times 96485\times \text{deposited Al (mol)}}{I\times t}\times 100 \tag{2}$$

The nominal thickness is calculated by Eq. 3:

$$\text{Nominal thickness } (\mu\text{m}) = \frac{\text{deposited Al(g)}/\rho_{\text{Al}}(\text{g/cm}^3)}{S(\text{area, cm}^2)}\times 10^4 \tag{3}$$

Results and Discussion

Electrical conductivities

For electrodeposition application, electrical conductivity is one of the most important properties of electrolyte. Electrolytes with higher conductivities will have lower Ohmic drop during electrolysis and thus lower cell voltage, higher energy efficiency and higher deposition rate would be expected. Besides, in developing ILs for practical applications, it will be necessary to accumulate much fundamental data on the solubility of metal compounds.

Because anionic species of $AlCl_3$/[bmim]Cl change with the molar ratio of $AlCl_3$ to [bmim]Cl, chemical and electrochemical properties of the melts change drastically with the composition. Therefore, we measured the conductivities of different molar ratio of $AlCl_3$ to [bmim]Cl (from 0.1:1 to 2.0:1) at 298 K. Figure 1 shows that the conductivity is markedly dependent upon composition of the electrolyte.

As shown in Figure 2a, the electrical conductivities increase with the temperature (298–358 K) as expected, because the viscosity of the electrolytes decreases and hence the mobility of the ions increases with the temperature. To further understand the temperature-dependent behavior of the conductivities, the logarithm of the conductivity (κ) as a function of the inverse of absolute temperature ($1/T$), ln κ vs. $1/T$ as seen in Figure 2b, was plotted on the basis of the Arrhenius equation[56]:

$$\kappa = A\ \exp\left(\frac{-E_a}{RT}\right) \tag{4}$$

In Eq. 4, κ is the electrical conductivity, A is a frequency factor based on the number of charge carriers, Ea is the activation energy, R is the gas constant and T is the absolute temperature.

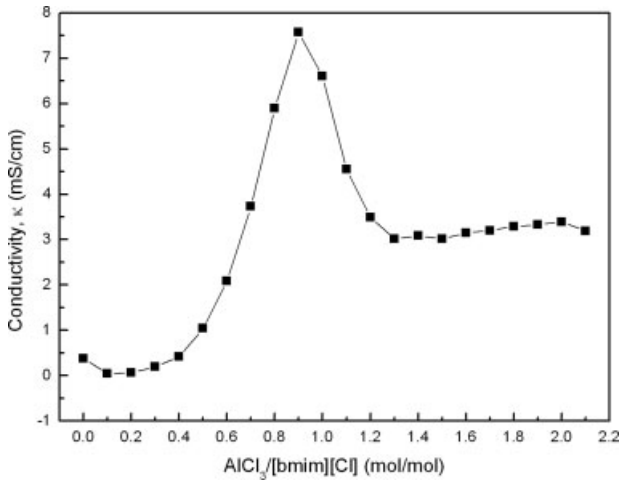

Figure 1. Electrical conductivities (κ) of the $AlCl_3$/[bmim]Cl electrolytes at 298 K as a function of molar ratio.

If the conductivity data would follow the Arrhenius behavior given by Eq. 2, the plot of ln κ vs. $1/T$ should be linear. Results in Figure 2b indicate that the temperature-dependent behavior of the conductivity can be correlated by the Arrhenius equation. The fit to the Arrhenius equation gave values of the parameter A and E_a. The activation energy for the conductivities was calculated to be 15.78 kJ/mol.

Effect of current density

Current density usually has a significant influence on the deposit brightness, thickness distribution, current efficiency and microstructure of the electrodeposits. Herein the effect of current density was investigated from 8 to 26 mA/cm^2 in 2.0:1 $AlCl_3$/[bmim]Cl at 318 K for 0.5 h in galvanostatic mode. The results suggested that the deposits are dense, adherent and homogeneous. In fact, the deposits formed at 14–24 mA/cm^2 are quite smooth and bright, and thus the optimum current densities were determined to be in this range. The current efficiency slightly decreases with increase in the current density in the range of 78.0–90.0%. The current efficiency decreases to be about 78.0% at 26 mA/cm^2. As the current density increases the total charge passed though the cell increases, hence the theoretical amount deposited also increases. However, the actual weight deposited does not follow a similar trend as that of current density due to the current loss (polarization effects) involved in electrolysis process. Therefore, lower current efficiencies can be attributed to the above phenomena.

It should be noted that higher current densities (>26 mA/cm^2) resulted in darker grey deposits with dendritic growth and poor adherence. Figure 3 shows the SEM micrographs of the deposits obtained in 2.0:1 $AlCl_3$/[bmim]Cl at 318 K for 0.5 h as a function of the current density (from 14 to 26 mA/cm^2). The deposits obtained at 14, 18, and 26 mA/cm^2 display similar microstructure (Figures 3a–d). Relatively rough surface with larger clusters of particles is observed on the deposits obtained at 26 mA/cm^2 (Figure 3d). The deposit obtained at 22 mA/cm^2 is denser, compacter and smoother, with smaller crystallites on the order of smaller than 10 μm (Figure 3c). From the analysis of the deposit microstructure at 318 K, it appears that the morphology of deposits was relatively independent of current density.

However, deposit microstructure obtained at higher temperature (348 K) of the electrolyte revealed interesting features as a function of current density. Figure 4 shows the SEM micrographs of Al coatings with a current density of 14–44 mA/cm^2 at 348 K. The deposits obtained at 14 and 22 mA/cm^2 display similar spiculate microstructure (Figures 4a, b), except that the former (Figure 4a) is much denser and more homogeneous and the growth of particles is observed for the latter (Figure 4b). At higher current densities a compact layer of deposit microstructure with spherical particles was observed as seen in Figures 4c, d. With the highest current density, particles in Figure 4d are a little smaller and more homogeneous than those in Figure 4c. It can be seen from the above microstructures that at 348 K, the type of

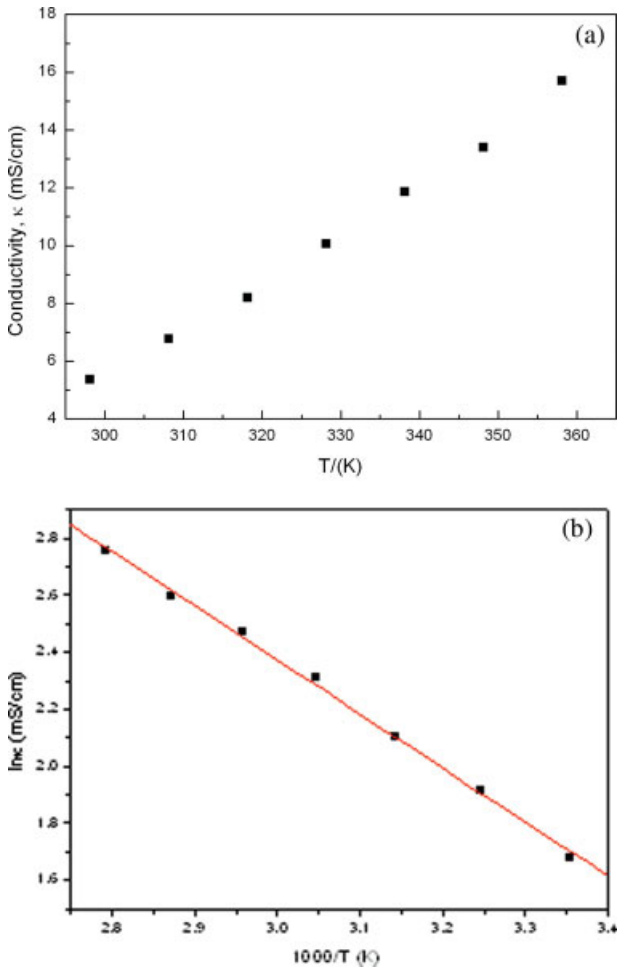

Figure 2. (a) Electrical conductivities (κ) of the $AlCl_3$/[bmim]Cl electrolytes (2.0:1 molar ratio) as a function of temperature. (b) ln κ vs. $1/T$, displays the linear Arrhenius behavior.

[Color figure can be viewed in the online issue, which is available at www.interscience.wiley.com.]

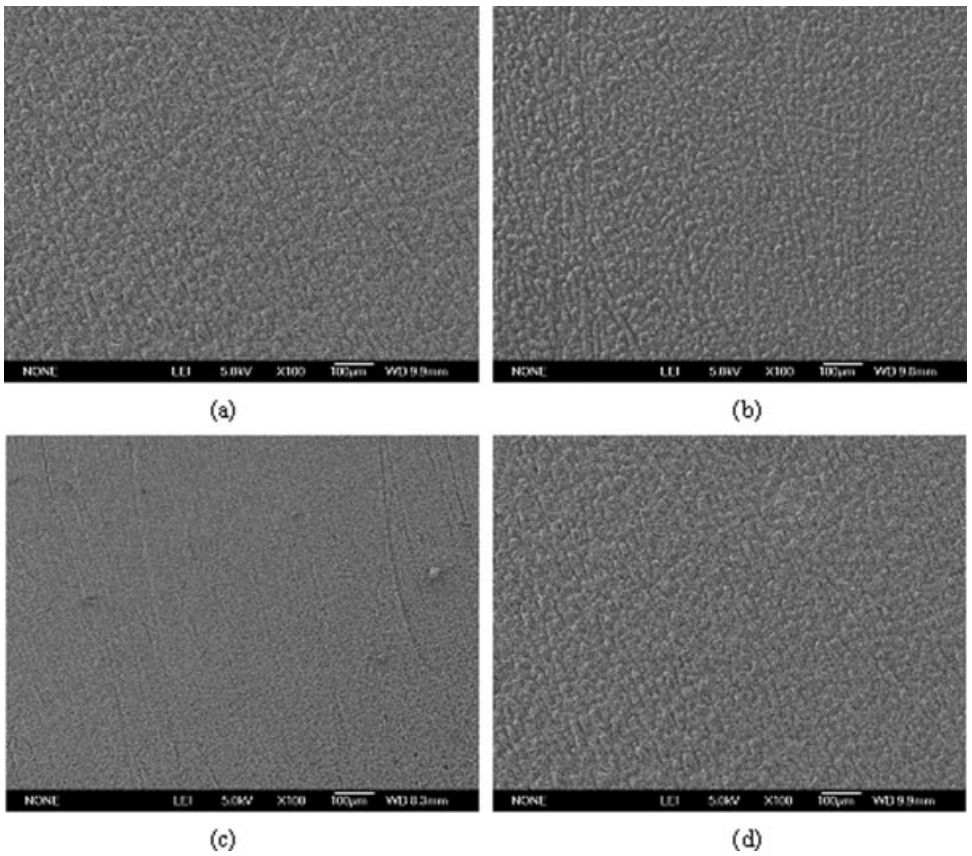

Figure 3. SEM micrographs of the aluminum coatings obtained from 2.0:1 $AlCl_3$/[bmim]Cl at 318 K for 0.5 h under stirring condition by magnetic stirrer (300 rpm) with different current densities (mA/cm^2).

(a) 14; (b) 18; (c) 22; (d) 26. Their nominal thicknesses are 7.83, 10.00, 11.25, and 12.60 μm, respectively.

deposit microstructure changed rapidly as a function of current density. Unlike the case of low temperature (318 K) where the deposit microstructure is relatively independent of current density, at 348 K, the influence of current density is clearly seen on the deposit microstructure. The combined influence of increased temperature and current density seems to have led to a nucleation-controlled microstructure. The color of gained Al coatings in 2.0:1 $AlCl_3$/[bmim]Cl at 348 K for 0.5 h were darker than ones obtained at 318 K in general. At 348 K, with the increase of the current density, the color gradually changed to darker grey. The current efficiencies decrease with increase in the current density in the range of 71.8–83.3%. Compared with the one gained at 318 K, the relationship between the current efficiency and current density at 348 K seems to be the same as that of 318 K.

Effect of temperature

As shown in section *electrical conductivitivities*, temperature has a significant effect on the conductivities of the $AlCl_3$/[bmim]Cl electrolytes. To determine the optimum operating temperatures, the effect of electrolyte temperature was investigated in 2.0:1 $AlCl_3$/[bmim]Cl at 22 mA/cm^2. It was found that almost silver gray or black deposits were formed at temperatures higher than 348 K. However, shining and homogeneous deposits were obtained at 298–348 K. The optimum temperatures were found to be in the range from 308 to 328 K, where smoother, denser and brighter deposits were obtained. With the increase of the temperature, the current efficiency increases first and then decreases to about 78.0%, including the maximum 82.3% got at 318 K. The supreme current density is remarkably enhanced by the increase of temperature, with 26 mA/cm^2 for 298 K and 46 mA/cm^2 for 348 K, respectively.

Figure 5 shows the SEM images of the deposits obtained in 2.0:1 $AlCl_3$/[bmim]Cl for 0.5 h at various temperatures with a current density of 22 mA/cm^2. The deposits obtained at 298 K, 308 K, and 318 K display similar microstructure with spherical particles (Figures 5a–c). With a temperature increase from 298 K to 318 K, the deposit is much denser and smoother, with the smallest crystallite on the order of smaller than 5 μm (Figure 5c). Relatively rough surface with larger clusters of particles is observed on the deposits obtained at 298 K and 308 K (Figures 5a, b). However, deposit microstructures obtained at higher temperature (from 328 K to 348 K) are quite different from those at lower temperature (from 298 K to 318 K). The deposits obtained at 328 K, 338 K, and 348 K display similar spiculate microstructure (Figures 5c–e), except that at lower temperatures the deposit microstructures are much denser and more homo-

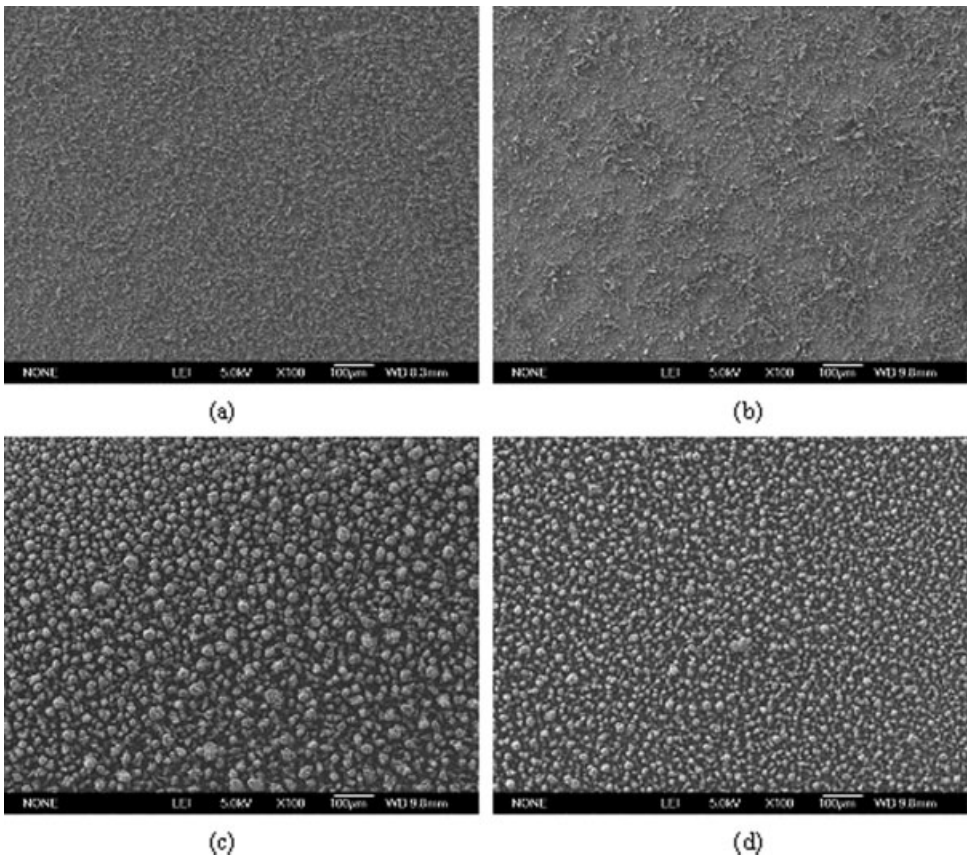

Figure 4. SEM micrographs of the aluminum coatings obtained from 2.0:1 $AlCl_3$/[bmim]Cl at 348 K for 0.5 h under stirring condition by magnetic stirrer (300 rpm) with different current densities (mA/cm^2).

(a) 14; (b) 22; (c) 34; (d) 44. Their nominal thicknesses are 7.25, 10.69, 15.56, and 19.63 μm, respectively.

geneous and the growth of particles is observed at higher temperatures. From the analysis of the deposit microstructure at different temperatures, it appears that the type of deposit microstructure changed rapidly as a function of temperature and the morphology of deposits was greatly dependent of temperature. The influence of increased temperature seems to have resulted in a nucleation-controlled microstructure.

Effect of molar ratio of $AlCl_3$/[bmim]Cl

The molar ratio of $AlCl_3$/[bmim]Cl is an important parameter that influences the reactions taking place at the electrodes. The effect of the molar ratio of $AlCl_3$/[bmim]Cl was investigated from 1.2:1 to 2.0:1 at 318 K for 0.5 h with a current density of 12 mA/cm^2 in the present study. Shining, dense and adherent deposits were formed with the molar ratio of $AlCl_3$/[bmim]Cl from 1.6:1 to 2.0:1. The current efficiency for the 1.4:1 $AlCl_3$/[bmim]Cl electrolyte was found to be 89.3% at 318 K and 12 mA/cm^2. For all other electrolytes with molar ratio from 1.6:1 to 2.0:1, the current efficiency was calculated to be about 90.0 $\pm$ 1% under the given conditions, indicating that the molar ratio of $AlCl_3$/[bmim]Cl has no significant influence on the current efficiency. Similar results were obtained for the nominal thickness. High molar ratio of $AlCl_3$/[bmim]Cl yielded high current densities. This is due to the increase in the number of ions of the electrolyte.[55]

Figure 6 shows the SEM images of the deposits obtained in different molar ratio of $AlCl_3$/[bmim]Cl at 318 K for 0.5 h with a current density of 12 mA/cm^2. In Figure 6a, with the molar ratio of 1.4:1, a deposit of spherical particles in a close size range of 10–20 μm can be observed where some amount of agglomeration of particles appears to have taken place. In Figure 6b, with molar ratio of 1.6:1, the deposit morphology reveals a dense and compact layer containing nonspherical particles formed as small clusters with an average size of 1–2 μm. As the molar ratio of the electrolyte increases further to 1.8:1, the deposit obtained was similar to that obtained at the molar ratio of 1.4 but with fine particles (average size of 1–3 μm). At the highest molar ratio (2.0:1) of the electrolyte the deposit depicted a dense spherical microstructure with an average particle size of 5–10 μm. It can be seen that the aluminium deposit microstructure has some dependence on the electrolyte composition. A nucleation-controlled deposit growth is evident from the analysis of deposit microstructure.

Effect of deposition time

The nominal thickness of the deposits is significantly related to the deposition time. To understand the relationship between electrodeposition time and the nominal thickness, the electro-

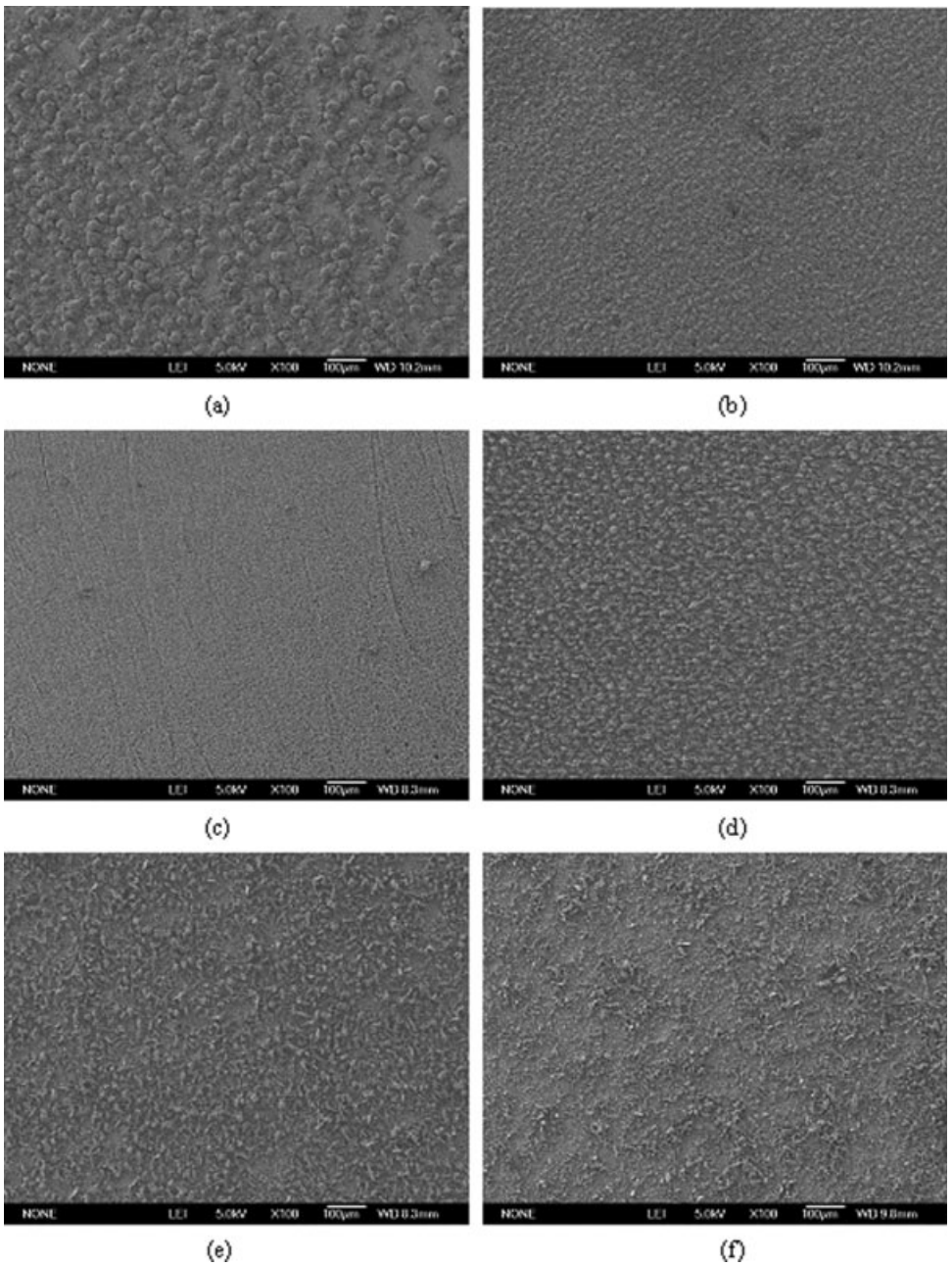

Figure 5. Surface morphologies of the aluminum deposits obtained from 2.0:1 $AlCl_3$/[bmim]Cl at 22 mA/cm^2 for 0.5 h under stirring condition by magnetic stirrer (300 rpm).

(a) 298 K; (b) 308 K; (c) 318 K; (d) 328 K; (e) 338 K; (f) 348 K. Their nominal thicknesses are 9.58, 10.27, 11.25, 11.12, 10.38, and 10.69 μm, respectively.

deposition time was investigated from 10 to 60 min under the same conditions (2.0:1 $AlCl_3$/[bmim]Cl at 318 K and 12 mA/cm^2 under stirring speed 300 rpm). As shown in Figure 7a, the nominal thicknesses increase with the deposition time as expected. Results in Figure 7b indicate that the plot of nominal thickness vs. $t^{1/2}$ is linear. The grain size increases from about 2 to 10 μm and the current efficiency falls from about 91.0 to the 78.0% along with the time extending. Appropriate deposition time should be determined on the basis of the all-around considerations, such as the nominal thickness, the current density, the grain size and so on.

Effect of stirring speed

It has been reported that surface morphology of aluminum alloys obtained in the Lewis acidic chloroaluminate melts is improved by stirring.[57,58] Therefore, to obtain the optimum stirring speed, electrolysis was conducted in 2.0:1 $AlCl_3$/

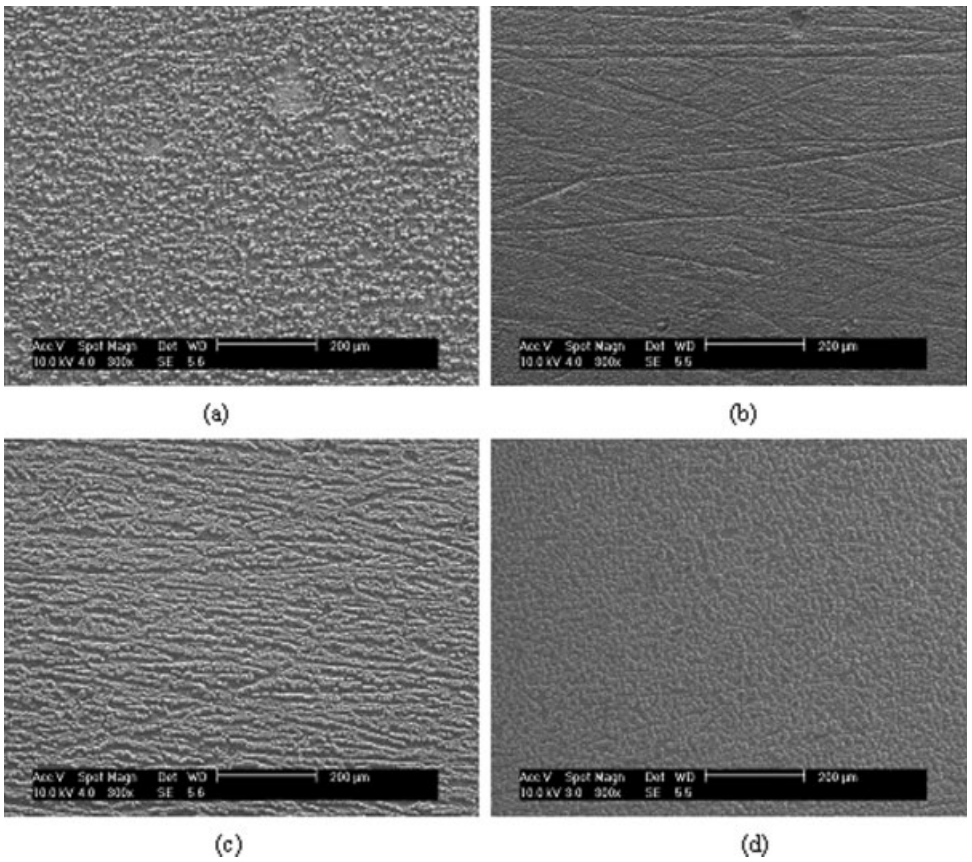

Figure 6. Surface morphologies of the aluminum deposits obtained from various ratios of $AlCl_3$/[bmim]Cl at 318 K and 12 mA/cm^2 for 0.5 h under stirring condition by magnetic stirrer (300 rpm).

(a) 1.4:1; (b) 1.6:1; (c) 1.8:1; (d) 2.0:1. Their nominal thicknesses are 6.67, 6.80, 6.77, and 6.74 μm, respectively.

[bmim]Cl for 0.5 h at 318 K with a current density of 22 mA/cm^2, stirring at the speed from 100 to 500 rpm. As shown in Figure 8, it appears that the surface morphology of deposits was relatively independent of stirring speed except that at higher stirring speeds (>300 rpm) the particle size is slightly increasing. However, the supreme current density is significantly enhanced by the increase of stirring speed. In addition, Lower stirring speed (<200 rpm) leads to smaller current density and higher stirring speed (>500 rpm) results in poor adherence to the substrate. Thus the optimum stirring speeds were determined to be in the range of 300–500 rpm. The nominal thickness and the current efficient increase with the advancement of the stirring speed from 9.40 to 12.29 μm and from 68.8 to 89.9%, respectively. This may result from that the faster of the stirring speed, the mass transfer is quicker and the deposited quantity is more.

Composition analysis and crystal structure of the electrodeposition film

The compositions of the samples electrodeposited under different conditions were determined by EDAX. Figure 9 show the EDAX analyses of the deposits obtained on the working electrodes after 0.5 h in 2.0:1 $AlCl_3$/[bmim]Cl at 318 K and 18 mA/cm^2, and at 348 K and 34 mA/cm^2, respectively. As expected, the deposits display a strong peak for aluminum, and relatively weak peaks of iron and oxygen. The Fe detected in the Al deposits may come from the substrate and the detected O may result from the oxidation of Al or Fe. Tables 1 and 2 show the components of the deposits clearly.

XRD pattern of the obtained samples shows only patterns of aluminum metal (Figure 10). Similar results are observed for other samples. The only difference from the JCPDS card is the ratio of peak intensities which will be discussed in the following.

Many experiments have been performed to study the influence of bath conditions, such as bath composition, current density, temperature, presence of impurities and brightening agents on the preferred orientation of almost every metal that can be electrodeposited. A general review was given by Pangarov.[59] The orientation of the obtained samples was studied by analyzing the results of XRD.[41,58] The normalized integrated intensity, P_{hkl}, for the (111), (200), (220), (311), and (222) reflections were calculated by using the following expression:

$$P_{hkl} = \frac{I_{hkl}/\sum I_{hkl}}{Ir_{hkl}/\sum Ir_{hkl}} \tag{5}$$

where I_{hkl} is the Peak intensity of the (*hkl*) reflection for the obtained samples; $\sum I_{hkl}$ is the sum of peak intensities for the

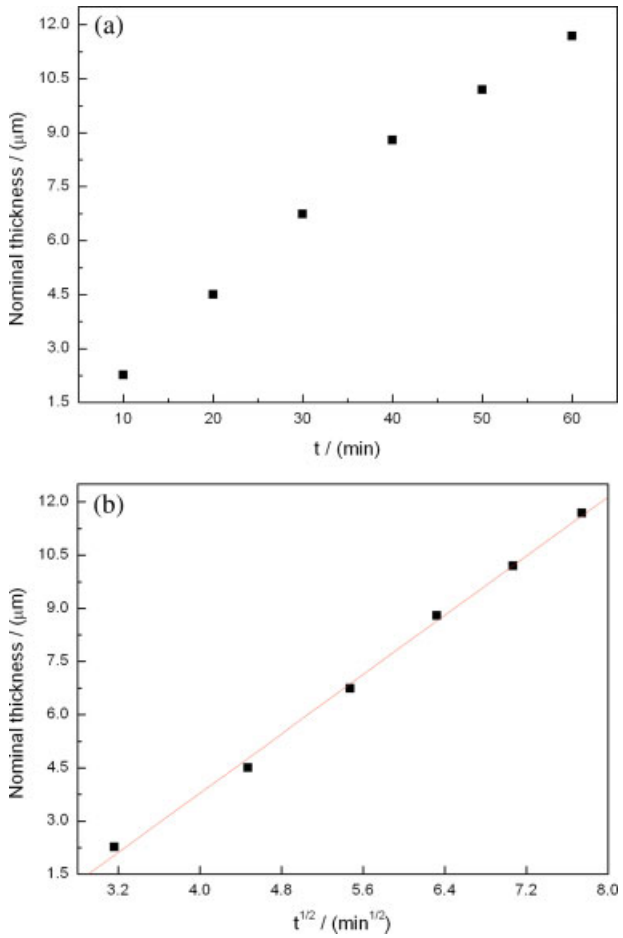

Figure 7. (a) Variation of the nominal thickness with deposit time in 2.0:1 $AlCl_3$/[bmim]Cl at 318 K and 12 mA/cm^2 under stirring speed 300 rpm; (b) nominal thickness vs. $t^{1/2}$, displays the linear behavior.

[Color figure can be viewed in the online issue, which is available at www.interscience.wiley.com.]

obtained samples; Ir_{hkl} is the peak intensity of the (hkl) reflection for the JCPDS card no. 01-089-2769 and $\sum Ir_{hkl}$ is the sum of peak intensities for the JCPDS card no. 01-089-2769.

The calculated results are plotted in Figures 11 and 12. It is shown in Figure 11 that all of the electrodeposits exhibited a preferred (200) crystallographic orientation except at 308 K and the strongest orientation of (200) is observed at 318 K, which shows that temperature has significant influence on the crystallographic orientation. Crystallographic orientations of electrodeposits obtained at 318 and 348 K with different current densities in Figure 12 show that there does not appear to be an apparent impact of current density on the crystallographic orientation. At 318 K, the (200) intensity was stronger than that of a randomly referenced oriented sample and the (111), (220), (311), and (222) reflections were relatively weak, though a slight increase in the (200) and decrease in the (111) intensities with increased current density were observed. On the other hand, at 348 K, the (111) intensity was essentially equal to that of a randomly referenced oriented sample. The (220), (311), and (222) reflections were relatively weak, though one does observe an increase in the (220) reflection at 34 mA/cm^2.

Nucleation and growth process for the electrodeposition of Al

The nucleation/growth process of aluminum in the $AlCl_3$/[bmim]Cl was investigated by means of chronoamperometry, which is an excellent choice for the study of the electrocrystallization mechanism because appropriate models can be used for the analysis of nucleation process.

In the chronoamperometric measurements, all experiments were conducted by stepping the potential of the working electrode from a value (usually the open-circuit potential) where no reduction of Al(III) would occur to those potentials sufficiently negative to initiate the nucleation/growth process. Shown in Figure 13 are a family of experimental current-time transients resulting from different step potentials for the electrodeposition process of Al on stainless steel electrodes in 2.0:1 $AlCl_3$/ [bmim]Cl at 298 K. As it could be seen, all of the current transients were of the same shape with well-defined current maxima. These transients show typical shape for a nucleation process. The current increased because of the nucleation and growth of the new phase and/or the increasing number of nuclei after the decay of double layer charging. After current maxima all the current transients decayed slowly reaching a constant value after about 150 s. The current is thought to reach maximum values, i_m, when the diffusion zones of the growing nuclei began to overlap.

The models describing the three-dimensional nucleation/growth processes during the bulk metal deposition on foreign substrate have been summarized by Allongue and Souteyrand.[60] Among them the models involving hemispherical diffusion-controlled growth of the nuclei[61] have been found to be suitable for representing metal deposition in most systems. The two limiting cases of this model are instantaneous nucleation and progressive nucleation. In general, a better method for distinguishing the two nucleation models is to compare the dimensionless experimental current-time transients with dimensionless theoretical transients for each nucleation mechanism,[61,62] which is given as follows:

For instantaneous nucleation,

$$\left(\frac{i}{i_m}\right)^2 = \frac{1.9542}{(t/t_m)}\left\{1-\exp\left[-1.2564\left(\frac{t}{t_m}\right)\right]\right\}^2 \qquad (6)$$

For progressive nucleation,

$$\left(\frac{i}{i_m}\right)^2 = \frac{1.2252}{(t/t_m)}\left\{1-\exp\left[-2.3367\left(\frac{t}{t_m}\right)\right]^2\right\}^2 \qquad (7)$$

These expressions correlate the dimensionless current (i/i_m) to the dimensionless time (t/t_m) for each nucleation model. The dimensionless plots, $(i/i_m)^2$ vs. (t/t_m) along with theoretical curves from Eq. 6 and 7, are shown in Figure 14. It is apparent that the dimensionless experimental data are in good agreement with the progressive three-dimensional diffusion controlled nucleation process described by Eq. 7 before the current maxima and the instantaneous three-dimensional diffusion controlled nucleation process described by Eq. 6

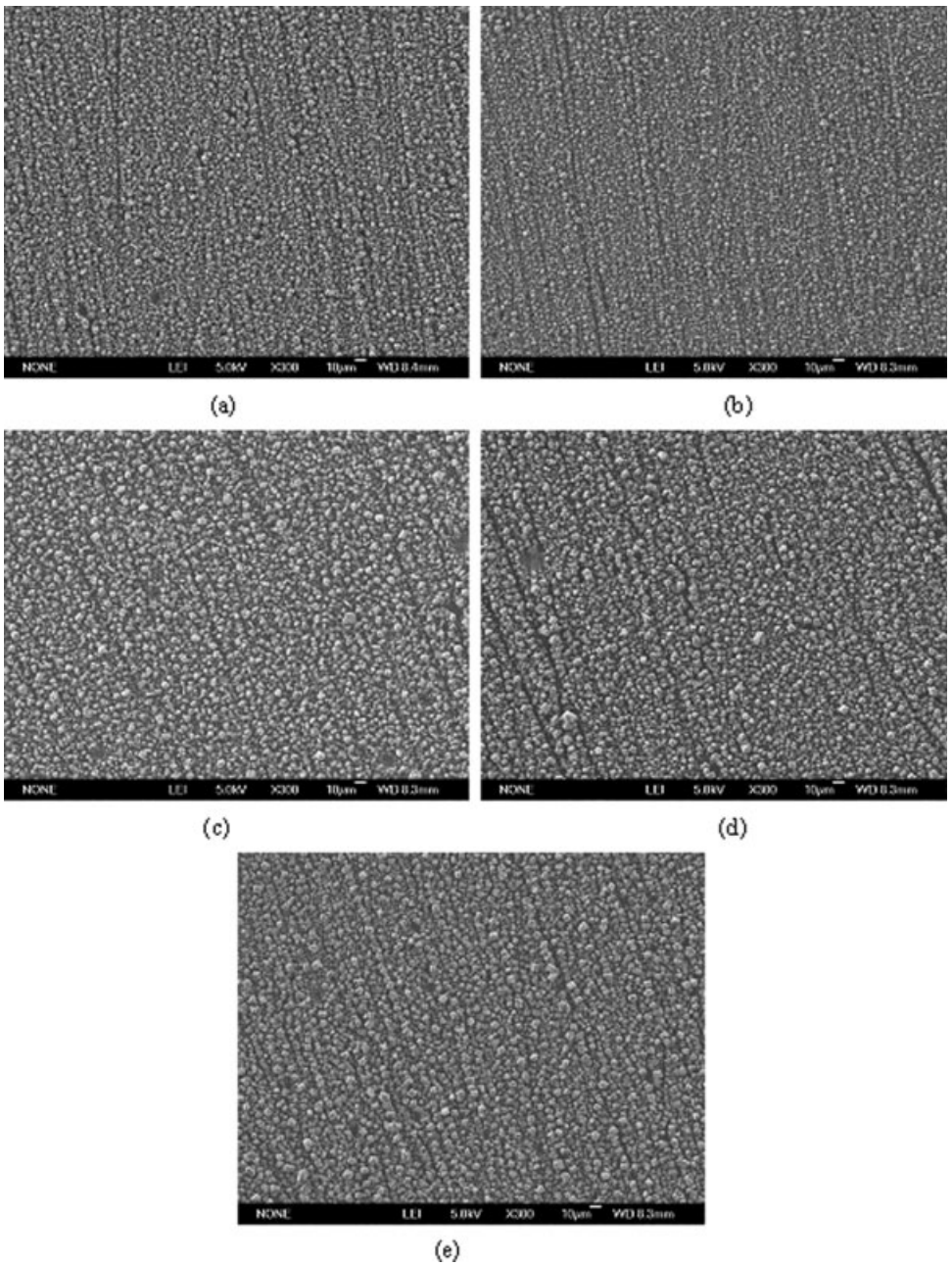

Figure 8. Surface morphologies of the aluminum deposits obtained from: 2.0:1 $AlCl_3$/[bmim]Cl for 0.5 h at 318 K with a current density of 22 mA/cm^2.

(a) 100 rpm; (b) 200 rpm; (c) 300 rpm; (d) 400 rpm; (e) 500 rpm. Their nominal thicknesses are 9.40, 10.87, 11.25, 11.78, and 12.29 μm, respectively.

after the current maxima. These results appear that there is a conversion from progressive to instantaneous in the three-dimension nucleational/growth on stainless steel.

Conclusions

It has been shown that a number of samples with silver white aluminium coating and well adherence to the substrates steel could be obtained by electrodeposition under different conditions in $AlCl_3$/[bmim]Cl. Some important factors, such as current density, temperature, molar ratio of $AlCl_3$/[bmim]Cl, stirring speed and deposition time do have effects on the alminium deposit brightness, thickness distribution and current efficiency of the electrolysis. The analysis shows that the electrical conductivities for $AlCl_3$/[bmim]Cl electrolyte can be well described by the Arrhenius equation. The results also show that the electrolyte can be used for the electrodeposition of Al over a wide range of temperature

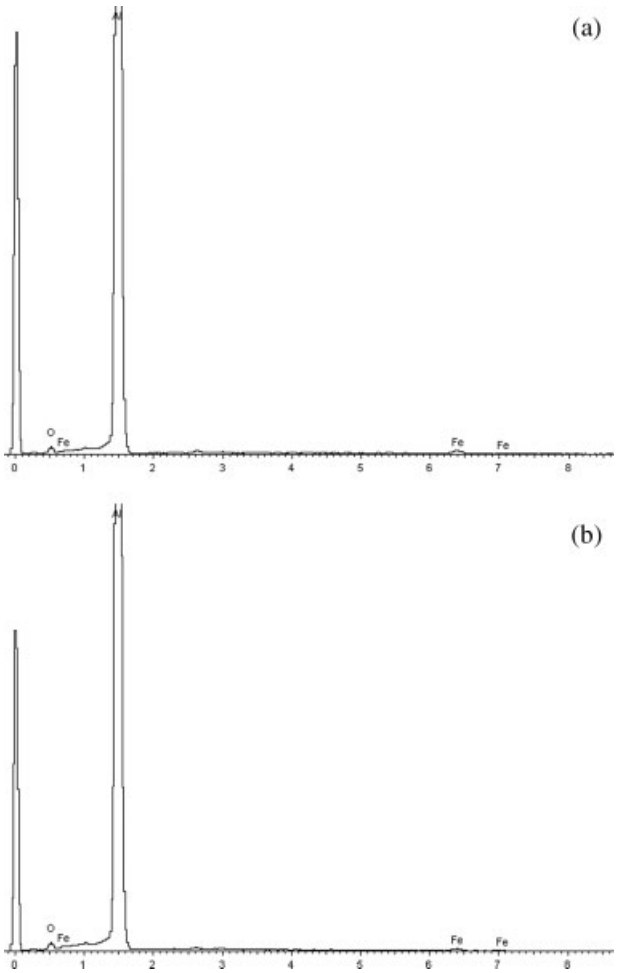

Figure 9. EDAX spectra of the deposit on cathode in 2.0:1$AlCl_3$/[bmim]Cl for 0.5 h.

(a) at 318 K and 18 mA/cm^2; (b) at 348 K and 34 mA/cm^2.

(298–348 K), current densities (8–44 mA/cm^2) and molar ratio (1.6:1–2.0:1). From the analysis of the deposit microstructure it appears that at low temperature (318 K) the morphology of aluminium deposit is relatively independent of current density. However, at higher temperature (348 K), the type of deposit microstructure changed rapidly as a function of current density. Results from the analysis of deposit microstructure at different temperatures show that the type of deposit microstructure changed rapidly as a function of temperature and the morphology of deposits was greatly dependent of temperature. Similar results can be obtained about the electrolyte composition. The cathodic current efficiency for Al

Table 1. Components of the Deposit in 2.0:1 $AlCl_3$/[bmim]Cl for 0.5 h at 318 K and 18 mA/cm^2

Element	Weight%	Atomic%
O K	2.35	3.94
Al K	95.79	95.16
Fe K	1.86	0.89
Totals	100.00	

Table 2. Components of the Deposit in 2.0:1 $AlCl_3$/[bmim]Cl for 0.5 h at 348 K and 34 mA/cm^2

Element	Weight%	Atomic%
O K	2.17	3.66
Al K	94.82	94.88
Fe K	3.01	1.46
Totals	100.00	

electrodeposition was nearly 70.0–90.0%. Results from electrolysis conducted at the speed from 100 to 500 rpm show that the surface morphology of deposits was relatively independent of stirring speed. The deposition time was investigated from 10 to 60 min and the relationship between nominal thickness and deposition time ($t^{1/2}$) was linear.

From the analysis of the experimental current transients, it was shown that the electrochemical deposition process of Al

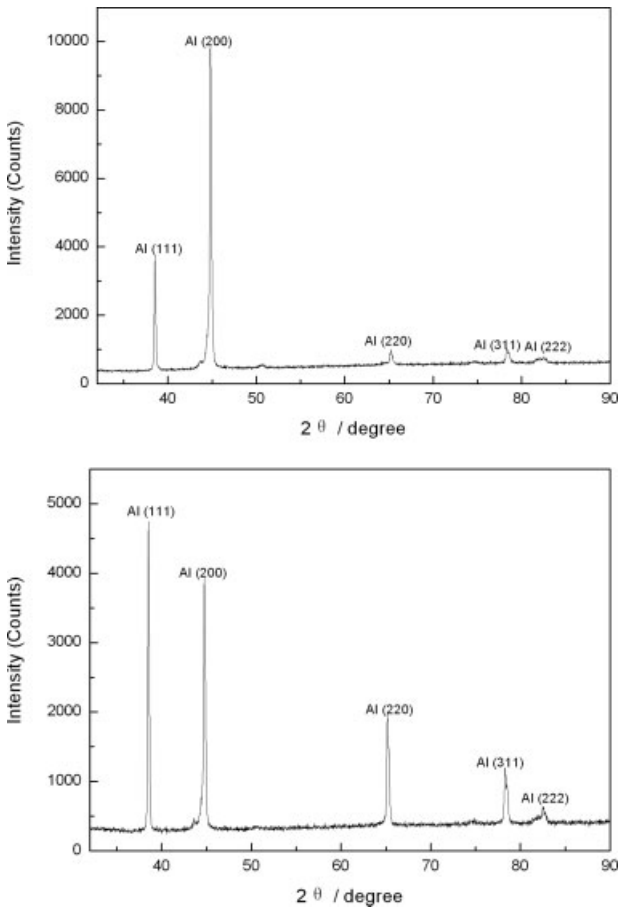

Figure 10. XRD pattern of electro-deposit Al on the stainless steel at galvano-static conditions (stainless steel plate as working electrode; Al plate as counter electrode; Al-wire as reference electrode; concentration ratio, 2.0:1 and time, 0.5 h).

(a) at 318 K and 18 mA/cm^2; (b) at 348 K and 34 mA/cm^2.

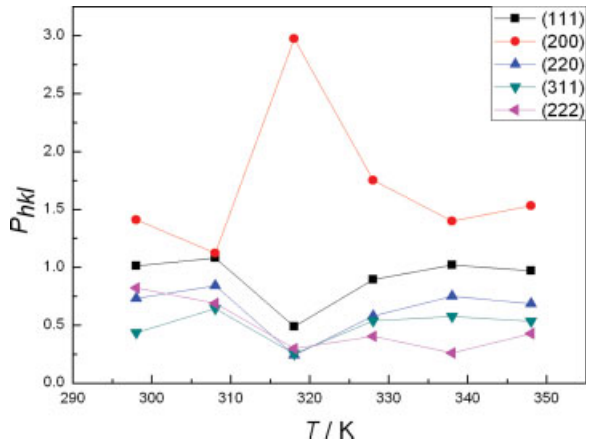

Figure 11. Normalized peak intensity, P_{hkl}, from XRD reflections of the samples obtained with a current density of 22 mA/cm^2 in 2.0:1 $AlCl_3$/[bmim]Cl for 0.5 h as a function of temperature.

[Color figure can be viewed in the online issue, which is available at www.interscience.wiley.com.]

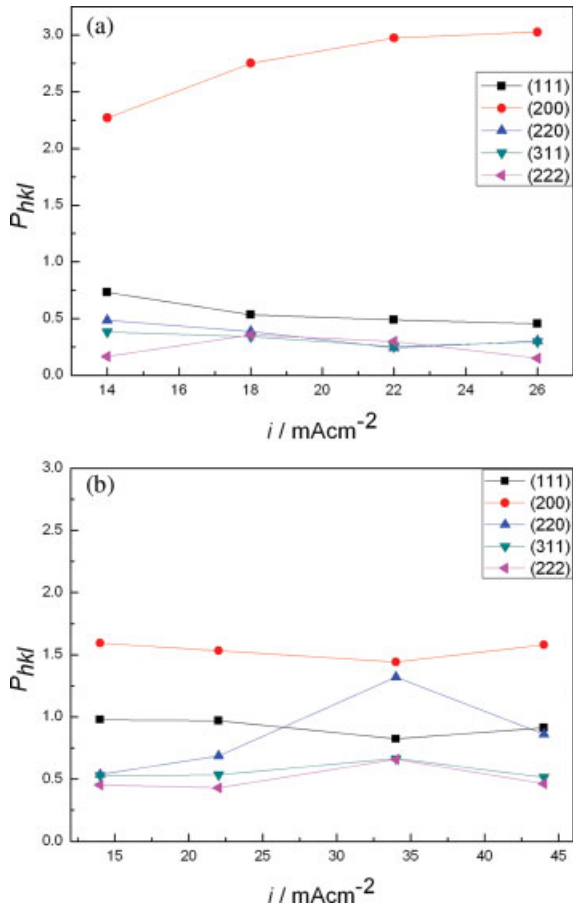

Figure 12. Normalized peak intensity, P_{hkl}, from XRD reflections of the samples obtained with different current densities in 2.0:1 $AlCl_3$/[bmim]Cl for 0.5 h.

(a) 318 K; (b) 348 K. [Color figure can be viewed in the online issue, which is available at www.interscience.wiley.com.]

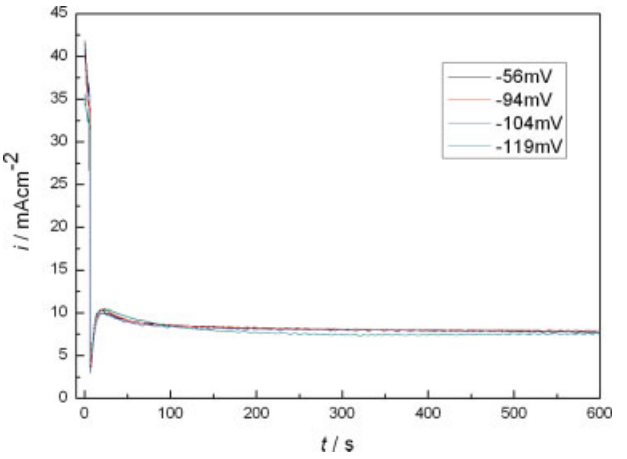

Figure 13. Chronoamperograms for a stainless steel electrode at various overpotentials in [bmim]Cl/$AlCl_3$ at 298 K.

(a) −56 mV, (b) −94 mV, (c) −104 mV, (d) −119 mV. [Color figure can be viewed in the online issue, which is available at www.interscience.wiley.com.]

in $AlCl_3$/[bmim]Cl was characteristic of three-dimension nucleation with diffusion-controlled hemispherical growth and there was a conversion from progressive nucleation to instantaneous nucleation: progressive nucleation before the current maxima and instantaneous nucleation after the current maxima. From the results of XRD, all of the electrodeposits exhibited a preferred (200) crystallographic orientation and the strongest orientation of (200) was observed at 318 K. It appears that there was not an apparent impact of current density on the crystallographic orientation of electrodeposits obtained at 318 and 348 K.

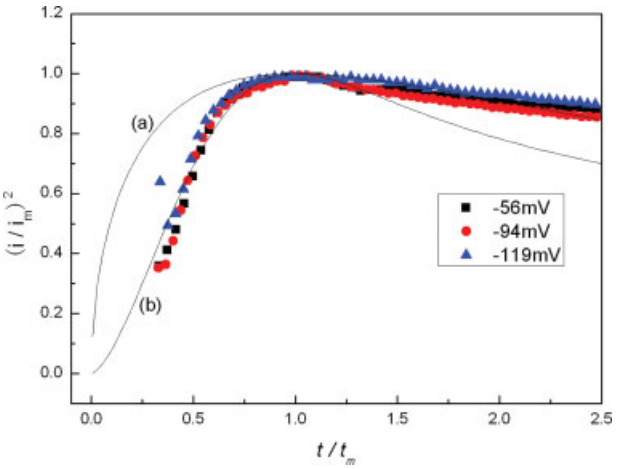

Figure 14. Comparison of dimensionless $(i/i_m)^2$ vs. (t/t_m) plots of nucleation/growth process on a stainless steel electrode at various overpotentials in [bmim]Cl/$AlCl_3$ at 298 K.

Theoretical models: (a) instantaneous and (b) progressive nucleation. Overpotentials: (■) −56 mV, (●) −94 mV, (▲) −119 mV. [Color figure can be viewed in the online issue, which is available at www.interscience.wiley.com.]

In summary, this work confirms that the novel approach developed in this study is a feasible and promising method for the electrodeposition of Al on stainless steel with a number of advantages such as substituting the volatile and flammable organic compounds and allowing the coating system with lower corrosivity and mild temperature. The easily adjusted deposit microstructure makes the process more attractive. Therefore, it can be expected that an Al electrodeposition process in ionic liquids has the potential to replace the present industrial procedure in the near future.

Acknowledgments

This work was supported financially by National Natural Science Foundation of China (Nos. 20776140 and 20873152), National Science Found for Distinguished Young Scholars of China (No.20625618), and National 863 Program of China (Nos. 2006AA06Z317 and 2006AA06Z371).

Literature Cited

1. Wang DQ, Shi ZY, Zou LJ. A liquid aluminum corrosion resistance surface on steel substrate. *Appl Surf Sci*. 2003;214:304–311.
2. Wang DQ, Shi ZY. Aluminizing and oxidation treatment of 1Cr18Ni9 stainless steel. *Appl Surf Sci*. 2004;227:255–260.
3. Paredes RSC, Amico SC, d'Oliveira ASCM. The effect of roughness and pre-heating of the substrate on the morphology of aluminium coatings deposited by thermal spraying. *Surf Coat Technol*. 2006;200:3049–3055.
4. Boogard A, van den Broek JJ. Crystallisation and electrical resistivity of sputter-deposited aluminium-germanium alloy films. *Thin Solid Films*. 2001;401:1–6.
5. Kersten H, Kroesen GMW, Hippler R. On the energy influx to the substrate during sputter deposition of thin aluminium films. *Thin Solid Films*. 1998;332:282–289.
6. Charrier C, Jacquot P, Denisse E, Millet JP, Mazille H. Aluminium and Ti/Al multilayer PVD coatings for enhanced corrosion resistance. *Surf Coat Technol*. 1997;90:29–34.
7. Yang D, Jonnalagadda R, Rogers BR, Hillman JT, Foster RF, Cale TS. Texture and surface roughness of PRCVD aluminum films. *Thin Solid Films*. 1998;332:312–318.
8. Gálová M. Electrodeposition of aluminium from organic aprotic solvents. *Surf Technol*. 1980;11:357–369.
9. Zhao YG, VanderNoot TJ. Electrodeposition of aluminium from nonaqueous organic electrolytic systems and room temperature molten salts. *Electrochim Acta*. 1997;42:3–13.
10. Ziegler K, Lehmkuhl H. Die elektrolytische abscheidung von aluminium aus organischen komplexverbindungen. *Z Anorg Allg Chem*. 1956;283:414–424.
11. Capuano GA, Davenport WG. Plating aluminum onto steel or copper from alkyl benzene electrolytes. *Plating*. 1973;60:251–255.
12. Peled E, Gileadi E. Electroplating of Al from aromatic hydrocarbons. *Plat Surf Finish*. 1975;62:342–347.
13. Legrand L, Tranchant A, Messina R. Behaviour of aluminium as anode in dimethylsulfone-based electrolytes. *Electrochim Acta*. 1994;39:1427–1431.
14. Legrand L, Tranchant A, Messina R. Electrodeposition studies of aluminum on tungsten electrode from $DMSO_2$ electrolytes. *J Electrochem Soc*. 1994;141:378–382.
15. Hirato T, Fransaer J, Celis JP. Electrolytic codeposition of silica particles with aluminum from $AlCl_3$-dimethylsulfone electrolytes. *J Electrochem Soc*. 2001;148:C280–C283.
16. Jiang T, Chollier Brym MJ, Dube G, Lasia A, Brisard GM. Studies on the $AlCl_3$/dimethylsulfone ($DMSO_2$) electrolytes for the aluminum deposition processes. *Surf Coat Technol*. 2007;201:6309–6317.
17. Couch DE, Brenner A. A hydride bath for the electrodeposition of aluminum. *J Electrochem Soc*. 1952;99:234–244.
18. Galinski M, Lewandowski A, Stepniak I. Ionic liquids as electrolytes. *Electrochim Acta*. 2006;51:5567–5580.
19. Connor JH, Brenner A. Electrodeposition of metals from organic solutions. *J Electrochem Soc*. 1956;103:657–662.
20. Ishibashi N, Yoshio M. Electrodeposition of aluminium from the NBS type bath using tetrahydrofuran–benzene mixed solvent. *Electrochim Acta*. 1972;17:1343–1352.
21. Yoshio M, Ishibashi N. High-rate plating of aluminium from the bath containing aluminium chloride and lithium aluminium hydride in tetrahydrofuran. *J Appl Electrochem*. 1973;3:321–325.
22. Siegfried B, Klaus S. US Patent 1983, 4,417,954.
23. Yoshio M. Electrodeposition of aluminum from nonaqueous solutions. *Met Finish*. 1987;85:33–38.
24. Altgeld W. Galvanic aluminum coating-an interesting alternative for electronics, optics and corrosion protection. *Metalloberfläche*. 1986; 40:253–255.
25. Godshall N. Molten salt metalliding of nickel alloys. *J Electrochem Soc*. 1976;123:137C–140C.
26. Nayak B, Misra MM. The electrodeposition of aluminium on brass from a molten aluminium chloride-sodium chloride bath. *J Appl Electrochem*. 1977;7:45–50.
27. Li JC, Nan SH, Jiang Q. Study of the electrodeposition of Al-Mn amorphous alloys from molten salts. *Surf Coat Technol*. 1998;106: 135–139.
28. Jafarian M, Mahjani MG, Gobal F, Danaee I. Electrodeposition of aluminum from molten $AlCl_3$-NaCl-KCl mixture. *J Appl Electrochem*. 2006;36:1169–1173.
29. Ueda M, Kigawa H, Ohtsuka T. Co-deposition of Al-Cr-Ni alloys using constant potential and potential pulse techniques in $AlCl_3$-NaCl-KCl molten salt. *Electrochim Acta*. 2007;52:2515–2519.
30. Jafarian M, Mahjani MG, Gobal F, Danaee I. Effect of potential on the early stage of nucleation and growth during aluminum electrocrystallization from molten salt ($AlCl_3$-NaCl-KCl). *J Electroanal Chem*. 2006;588:190–196.
31. Endres F. Ionic Liquids: solvents for the electrodeposition of metals and semiconductors. *ChemPhysChem*. 2002;3:144–154.
32. Hurley FH, Wier TP. The electrodeposition of aluminum from nonaqueous solutions at room temperature. *J Electrochem Soc*. 1951;98: 207–212.
33. Welch BJ, Osteryoung RA. Electrochemical studies in low temperature molten salt systems containing alumnium chloride. *J Electroanal Chem*. 1981;118:455–466.
34. Lipsztajn M, Osteryoung RA. Increased electrochemical window in ambient temperature neutral ionic liquids. *J Electrochem Soc*. 1983; 130:1968–1969.
35. Lai PK, Skyllas-Kazacos M. Electrodeposition of aluminium in aluminium chloride/1-methyl-3-ethylimidazolium chloride. *J Electroanal Chem*. 1988;248:431–440.
36. Stafford GR. The Electrodeposition of an aluminum-manganese metallic glass from molten salts. *J Electrochem Soc*. 1989;136:635–639.
37. Carlin RT, Crawford W, Bersch M. Nucleation and morphology studies of aluminum deposited from an ambient-temperature chloroaluminate molten salt. *J Electrochem Soc*. 1992;139:2720–2727.
38. Moffat TP. Electrodeposition of Al-Cr metallic glass. *J Electrochem Soc*. 1994;141:L115–L117.
39. Yang CC. Electrodeposition of aluminum in molten $AlCl_3$-n-butylpyridinium chloride electrolyte. *Mater Chem Phys*. 1994;37:355–361.
40. Zhao YG, VanderNoot TJ. Electrodeposition of aluminium from room temperature $AlCl_3$-TMPAC molten salts. *Electrochim Acta*. 1997;42:1639–1643.
41. Liao Q, Pitner WR, Stewart G, Hussey CL, Stafford GR. Electrodeposition of aluminum from the aluminum chloride-1-methyl-3-ethylimidazolium chloride room temperature molten salt + benzene. *J Electrochem Soc*. 1997;144:936–943.
42. Abbott P, Eardley CA, Farley NRS, Pratt A. Novel room temperature molten salts for aluminium electrodeposition. *Trans Inst Met Finish*. 1999;77:26–28.
43. Lee JJ, Bae IT, Scherson DA, Miller B, Wheeler KA. Underpotential deposition of aluminum and alloy formation on polycrystalline gold electrodes from $AlCl_3$/EMIC room-temperature molten salts. *J Electrochem Soc*. 2000;147:562–566.
44. Abbott AP, Eardley CA, Farley NRS, Griffith GA, Pratt A. Electrodeposition of aluminium and aluminium/platinum alloys from $AlCl_3$/benzyltrimethylammonium chloride room temperature ionic liquids. *J Appl Electrochem*. 2001;31:1345–1350.
45. Tsuda T, Hussey CL, Stafford GR. Electrodeposition of Al-Mo alloys from the Lewis acidic aluminum chloride-1-ethyl-3-methyli-

midazolium chloride molten salt. *J Electrochem Soc*. 2004;151: C379–C384.
46. Jiang T, Brym MJC, Dube G, Lasia A, Brisard GM. Electrodeposition of aluminium from ionic liquids. I. Electrodeposition and surface morphology of aluminium from aluminium chloride ($AlCl_3$)-1-ethyl-3-methylimidazolium chloride ([EMIm]Cl) ionic liquids. *Surf Coat Technol*. 2006;201:1–9.
47. Carlin RT, Osteryoung RA. Aluminum anodization in a basic ambient temperature molten salt. *J Electrochem Soc*. 1989;136:1409–1415.
48. Melton TJ, Joyce J, Maloy JT, Boon JA, Wilkes JS. Electrochemical studies of sodium chloride as a Lewis buffer for room temperature chloroaluminate molten salts. *J Electrochem Soc*. 1990;137:3865–3869.
49. Wilkes JS, Levisky JA, Wilson RA, Hussey CL. Dialkylimidazolium chloroaluminate melts: a new class of room-temperature ionic liquids for electrochemistry. *Inorg Chem.* 1982;21:1263–1264.
50. Endres F, Bukowski M, Rolf Hempelmann, Natter H. Electrodeposition of nanocrystalline metals and alloys from ionic liquids. *Angew Chem Int Ed Engl*. 2003;42:3428–3430.
51. Aravinda CL, Burger B, Freyland W. Nanoscale electrodeposition of Al on n-Si(1 1 1) : H from an ionic liquid. *Chem Phys Lett*. 2007;434:271–275.
52. Abbott AP, McKenzie KJ. Application of ionic liquids to the electrodeposition of metals. *Phys Chem Chem Phys*. 2006;8:4265–4279.
53. Auborn JJ, Barberio YL. An ambient temperature secondary aluminum electrode: its cycling rates and its cycling efficiencies. *J Electrochem Soc*. 1985;132:598–601.
54. Zell CA, Endres F, Freyland W. Electrochemical in situ STM study of phase formation during Ag and Al electrodeposition on Au(111) from a room temperature molten salt. *Phys Chem Chem Phys*. 1999;1:694–704.
55. Kamavaram V, Mantha D, Reddy RG. Recycling of aluminum metal matrix composite using ionic liquids: effect of process variables on current efficiency and deposit characteristics. *Electrochim Acta*. 2005;50:3286–3295.
56. Bansal D, Cassel F, Croce F, Hendrickson M, Plichta E, Salomon M. Conductivities and transport properties of gelled electrolytes with and without an ionic liquid for Li and Li-ion batteries. *J Phys Chem B*. 2005;109:4492–4496.
57. Matsunaga M, Morimitsu M, Nagano M, Tsuda T. Electrodeposition mechanism of amorphous aluminum alloys from chloroaluminate melts. *Molten Salt Forum*. 1998;5–6:601–604.
58. Tsuda T, Nohira T, Ito Y. Nucleation and surface morphology of aluminum-lanthanum alloy electrodepsited in a $LaCl_3$-saturated $AlCl_3$-EtMeImCl room temperature molten salt. *Electrochim Acta*. 2002;47:2817–2822.
59. Pangarov NA. Preferred orientations in electrodeposited metals. *J Electrochem Soc*. 1965;9:70–85.
60. Allongue P, Souteyrand E. Metal electrodeposition on semiconductors. I. Comparison with glassy carbon in the case of platinum deposition. *J Electroanal Chem.* 1990;286:217–237.
61. Scharifker B, Hills G. Theoretical and experimental studies of multiple nucleation. *Electrochim Acta*. 1983;28:879–889.
62. Lee JJ, Miller B, Shi X, Kalish R, Wheeler KA. Aluminum deposition and nucleation on nitrogen-incorporated tetrahedral amorphous carbon electrodes in ambient temperature chloroaluminate melts. *J Electrochem Soc*. 2000;147:3370–3376.

Manuscript received Dec. 18, 2007, and revision received Sept. 5, 2008.